Available online at www.sciencedirect.com
SCIENCE DIRECT
Sensors and Actuators A 127 (2006) 248–254
SENSORS AND ACTUATORS A PHYSICAL
www.elsevier.com/locate/sna

Micro vertical comb actuators by selective stiction process

Jongbaeg Kim [a,*], Dane Christensen [b], Liwei Lin [b]

[a] School of Mechanical Engineering, Yonsei University, 134 Shinchon-Dong, Seodaemun-Ku, Seoul 120-749, South Korea
[b] Berkeley Sensor and Actuator Center, University of California, Berkeley, CA 94720, USA

Received 1 March 2005; received in revised form 18 July 2005; accepted 8 August 2005
Available online 30 September 2005

Abstract

Selective stiction has been successfully applied to the batch fabrication of angular vertical comb actuators made of single-crystal silicon with self-aligned comb sets. The possible failure modes of the devices during the manufacturing process are studied, and a novel design of stiction plate and mechanical spring is also presented to suppress the failure modes. The fabrication process with unique designs of mechanical springs enables the stiction of microstructures in a controlled manner and significantly reduces unwanted compliances on the actuators, preventing unwarranted motion and providing stable operations. The prototype microactuators operate at a resonant frequency of 0.92 kHz with 85° optical scanning angle and quality factor of 162 in air under driving voltages of 19 V_{dc} plus 15 V_{pp}. A reliability test on an unpackaged actuator with more than 800 million cycles of operation showed extremely small variation in the resonant frequency and scanning angle, showing no sign of degradation in the induced stiction interface or the microstructures. Applications include scanning micromirrors, optical switches, and variable capacitors and we present results obtained with MEMS scanning mirrors.

Keywords: Actuator; Vertical comb; Stiction; Scanning mirror

1. Introduction

Electrostatic comb-drive actuators have been used in numerous MEMS applications for advantages in extended ranges-of-movement, stable and reliable operation, and design flexibility. In particular, optical MEMS applications have employed comb-drive actuators for out-of-wafer-plane torsional motions using vertically aligned comb-drives to achieve both higher frequencies and larger motions. Previous works have included vertically aligned comb-drives using the techniques of either polysilicon-on-SOI [1] or single-crystal silicon with wafer bonding [2]. These techniques commonly face the requirement of placing two sets of comb structures at different vertical positions, and precise alignment of the upper and lower combs during the fabrication process can be challenging. A self-aligned vertical comb design has been demonstrated previously [3], yet its fabrication process requires wafer-bonding, grinding, and polishing as well as silicon-anisotropic-etching. Reflow of polymer hinges was used to suppress the complexity of the fabrication process, in which the control and reliability of polymer material properties was a challenge [4]. Deflecting one side of comb structures using the residual stress induced by additional metal layer [5] has also been developed with a limitation of low frequency operation due to the very flexible structures to allow appreciable deformation. Alternatively, vertically self-aligned comb actuators fabricated by self-aligned plastic deformation of silicon under global heating [6] and localized heating [7] were demonstrated with large torsional scanning angles and good reliability. However, these methods require an additional plastic deformation process with microstructures on a separate protrusion wafer.

We present in this paper a simple solution to make self-aligned vertical comb actuators by applying the stiction phenomenon, which is generally undesirable in MEMS processing, to a critical manufacturing solution. Stiction (or auto-adhesion) in MEMS are distinguished into two types [8]: the process-related adhesion during the releasing process and the operation-related adhesion after the deployment of the device. The first is mainly due to the capillary forces from the post-release, rinse-dry cycle [9], which may significantly reduce the device yield. The second class occurs due to the overrange of the device motion or instability resulting direct contact of the surfaces during device operation [8,10].

* Corresponding author. Tel.: +82 2 2123 2810; fax: +82 2 312 2159.
E-mail address: kimjb@yonsei.ac.kr (J. Kim).

0924-4247/$ – see front matter © 2005 Elsevier B.V. All rights reserved.
doi:10.1016/j.sna.2005.08.035

We intentionally introduce process-related stiction on the designated microstructures to form initial angular displacement between the two comb sets of stator and rotor. The design for the actuators and selective stiction process [11] is discussed in the next section followed by fabrication, inspection and experimental evaluations of the actuator performance and reliability.

2. Design and fabrication

2.1. Principle

The critical point CO_2 drying process involves two key steps; first, liquid solvents such as methanol or IPA (Isopropyl Alcohol) are displaced with high-pressure liquid CO_2 and second, temperature is raised above the critical point of CO_2. Ideally, liquid–solid interface is never formed during the process to suppress capillary forces and prevent the stiction problem. The size of the gaps and tortuosity of the microstructures can affect the liquid-exchange processes. Highly tortuous pathways with small gaps could require longer time for the diffusion process to complete or stiction may occur due to residual non-CO_2 liquid [12]. We utilize this feature-dependent characteristic to achieve selective stiction.

Fig. 1 shows schematically how, in our process, selective stiction is applied to construct self-aligned vertical comb-sets using a SOI wafer with an initial, pre-determined tilt angle. The stiction-plate is connected to the fixed anchor through two mechanical springs that are flexible only in the out-of-plane direction. During the drying process, stiction-plates are designed to stick down to the substrate due to their relatively large surface area, resulting the height difference between the anchor and stiction-plate to generate the initial angular displacement of the rotor to accomplish the electrostatically actuated vertical actuator.

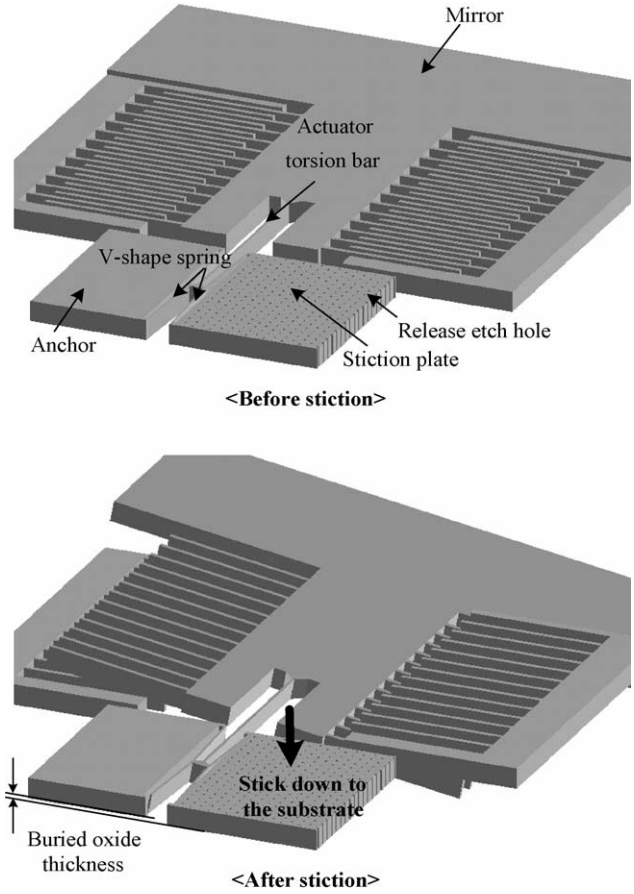

Fig. 1. Working principle of vertical comb actuators.

2.2. Process design

In Fig. 2, a two-mask fabrication process is presented. The comb actuators, mirror plates and stiction-plates are defined on the 50 μm-thick device layer of the SOI wafer in Fig. 2a. The buried oxide thickness is 1 μm. The backside patterning/etching of the substrate wafer underneath the mirror and comb sets provides clearance for the mirror motion. After etching both front and back sides of the wafer (b), the device layer is released in HF (c). Since there are array of etch holes on the stiction-plates, they are completely released from the substrate but connected to the main device structures via the mechanical springs. In the following drying process (d), the stiction-plate is stuck down, while other structures are completely released without stiction. In the process step (d), Tousimis® model 815 dryer was used with the purging time of 5 min and 10 sliced, 1 cm^2 pieces were concurrently processed in a Teflon® tray. Each piece contains 6–8 scanning mirror devices depending on the design variations. It is found that this time window gives best fabrication results that stiction-plate with large area of 1.26 mm^2 and evenly distributed etch holes of 4×4 μm^2 with 23 μm pitch will stick to the substrate.

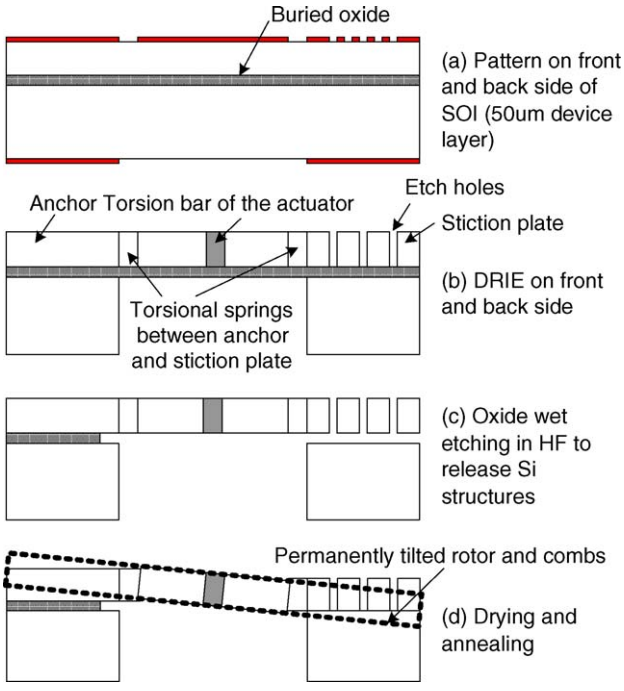

Fig. 2. Fabrication process flow (the buried oxide thickness and the tilting of the structure is exaggerated to illustrate the effect).

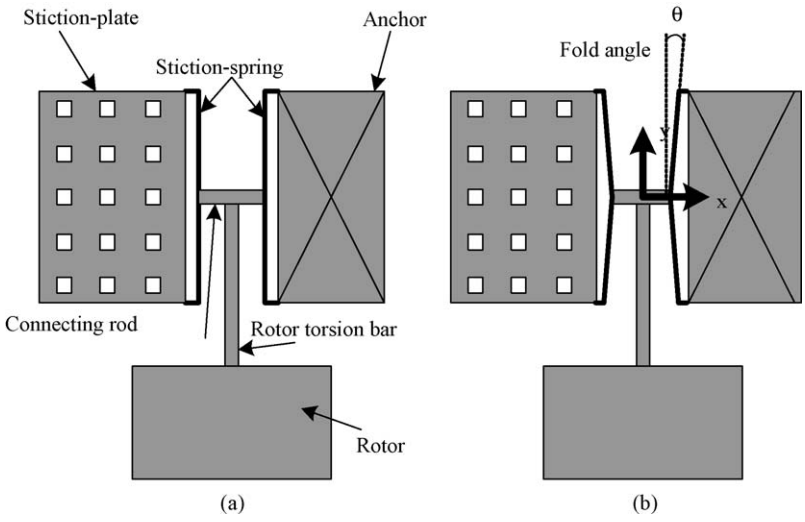

Fig. 3. Two different spring designs for stiction-plate.

The mechanical springs attached to the stiction-plate could allow only vertical motion, and the original locations of the stiction-plates are held to maintain self-alignment between the rotor and the stator comb sets. The stiction is believed to be permanent although an additional annealing at 900 °C can further enhance the bonding between the stiction-plate and the substrate.

2.3. Stiction-plate springs and actuator

The stiction-plate springs must be flexible in the out-of-substrate direction to allow stiction to occur but rigid in the in-plane direction without affecting the self-alignment of stator and rotor comb sets. Furthermore, the springs could be stiff enough to have minimum impact on the actuator performance such as resonant frequency and operational stability.

Fig. 3 illustrates two different stiction-spring designs we fabricated and tested. The basic structure consists of a pair of beams that are attached to stiction-plate and anchor, one connecting rod connecting the two beams, and a torsion bar connection to the rotor. The difference in (a) and (b) is that a fold angle, θ, is introduced in the stiction-spring design in (b) and we observed performance differences during the fabrication and testing stages. Specifically, the fold angle design enhances the structural rigidity in the x direction to prevent the

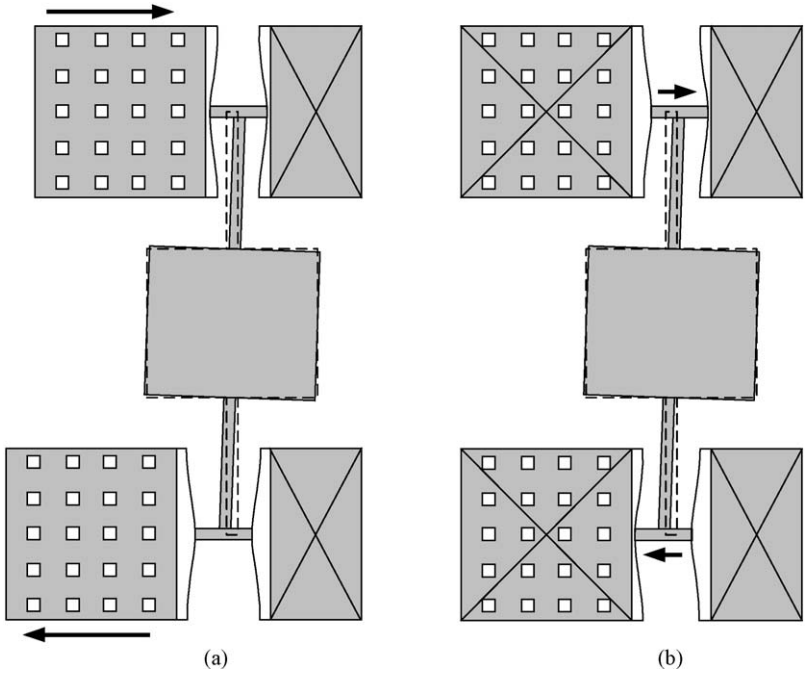

Fig. 4. Two possible failure modes of the actuators with insufficient rigidity of the stiction-spring design: (a) misplacement of the stiction-plate during the drying process due to lack of in-plane rigidity; (b) in-operation failure due to lack of in-plane rigidity such that under high operation voltage the rotor could rotate around the axis normal to the wafer plane as shown.

movement of rotor during the self-aligned deformation/stiction process.

Fig. 4 depicts two possible failure modes of the vertical comb actuators with the design in Fig. 3a: (1) the stiction-plate is misplaced during the stiction process due to the lack of the in-plane stiffness as illustrated in Fig. 4a where the worst case happen that the two stiction-plates move to opposite directions and cause the rotation of the rotor. The actuator failed to operate because the moving- and fixed comb sets are misaligned. (2) Another problem could happen during operation if the plate spring is not rigid. The whole rotor could rotate around the axis normal to the wafer plane as shown in Fig. 4b when the operation voltage is increased resulting the contact of moving- and fixed comb sets.

In Fig. 5 is the stiffness of the stiction-spring in two different directions with respect to the fold angle. The in-plane stiffness is the stiffness in the x direction and the vertical stiffness is in the out-of-wafer-plane direction. The stiffness values are calculated by FEA (Finite Element Analysis) and the stiction-spring is composed of a pair of two $4 \times 200\,\mu m^2$ beams with $50\,\mu m$ in thickness forming small fold angle between 0 and 7° and a connecting rod with $40\,\mu m$ length. As shown, the in-plane stiffness increases as the fold angle increases. On the other hand, the vertical stiffness that is desired to be as small as possible to allow the stiction-plate to stick, remains small. This vertical stiffness of the stiction-spring is inversely proportional to the length of the connecting rod, and can be reduced further by increasing the length of the connecting rod without affecting the in-plane stiffness. In the prototype device, we have chosen a fold angle of 3.6° as the starting point to investigate the device performance and improved yield and reduced failure rate have been achieved as compared with the ones with zero fold angle.

Fig. 6 shows the final layout of the stiction-plate with folded stiction-spring design, actuator torsion bar and the rotor of actuator including the mirror. The stiction-plate combination has one stiction-plate and two anchors that prevent the movement in x and y directions. Stiction of the stiction-plate causes the deformation of the stiction-spring and rotation of the connecting rod and the rotor. This initial tilt angle of the rotor is decided by thickness of the buried oxide and the length of the connecting rod. The detail dimensions of the prototype device are presented in Table 1.

Table 1
Detail dimensions of the actuator designed

Component	Dimension
Torsion bar	$7 \times 1000\,\mu m^2$
Mirror	$1000 \times 1200\,\mu m^2$
Comb finger size	$10 \times 250\,\mu m^2$ (overlap length: 220 μm, gap between fingers: 10 μm)
Number of comb fingers (double side actuation)	100
Etch hole size	$4 \times 4\,\mu m^2$
Etch hole pitch	23 μm
Each stiction-plate area	$1.26\,mm^2$
Stiction-spring	Two $4 \times 200\,\mu m^2$ bars form 3.6° fold angle

The stiction-spring introduces additional compliance to the whole rotor, and we evaluated this effect by conducting modal analysis as shown in Fig. 7. The mode shapes and the corresponding frequencies are shown. The values in the parentheses are the frequencies of the same rotor without using the stiction-spring design, i.e. the connecting rod is attached to the anchor and stiction-plate directly. It is found that the design with the stiction-spring has slightly lower modal frequencies.

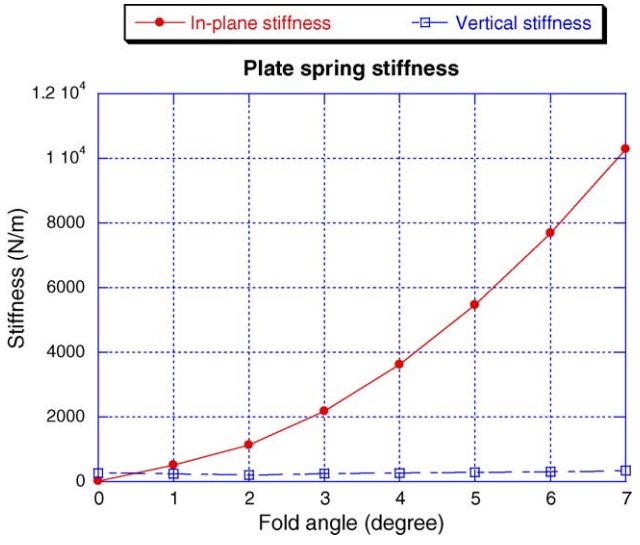

Fig. 5. In-plane (x-direction) and vertical (out-of-wafer-plane) stiffness of the folded stiction-spring as a function of fold angle calculated by FEA (Finite Element Analysis).

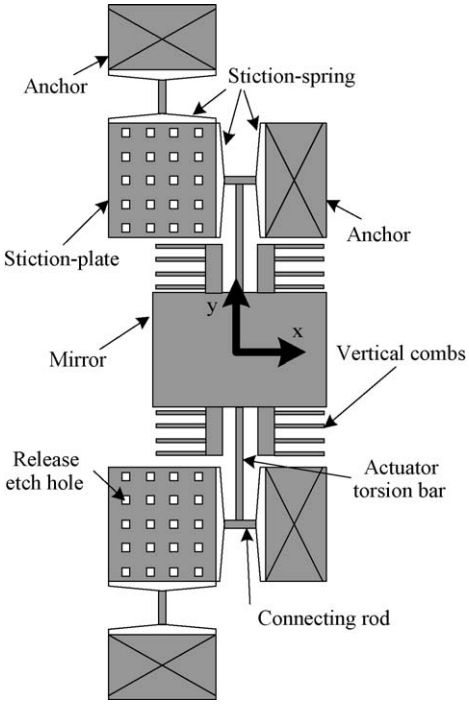

Fig. 6. Layout of the stiction-plate, stiction-spring with a fold angle, torsion bar and the rotor of actuator with mirror.

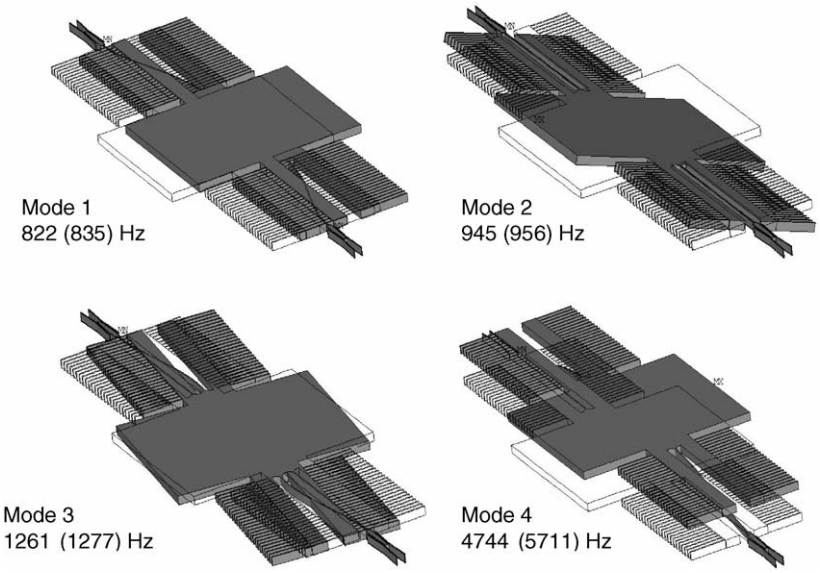

Fig. 7. Modal analysis and frequency comparison of the rotor with and without (in the parentheses) stiction-spring.

3. Fabricated devices

We used two different specifications of SOI wafers to fabricate the actuators using the same layout design shown in Table 1. The first one has 20 μm-thick device layer and 2 μm-thick buried oxide layer, while the second has 50 μm-thick device layer and 1 μm-thick buried oxide layer. Using the same fabrication process stated in the preceding section, the devices on the thin SOI sometimes showed non-uniform stiction, due to the bending of the stiction-plate. This in turn results smaller initial tilt angle than the designed value. On the other hand, the fabrication results on tilt angle for the thicker SOI devices are consistent with the designed values.

In Fig. 8, SEM pictures of the batch-fabricated actuators on 50 μm SOI are shown. The stiction-plates were lifted up forcefully to test the bonding strength. As shown in Fig. 9, this pull test always broke the stiction-plate implying good bonding strength. Fig. 10 shows a white light interferomet-

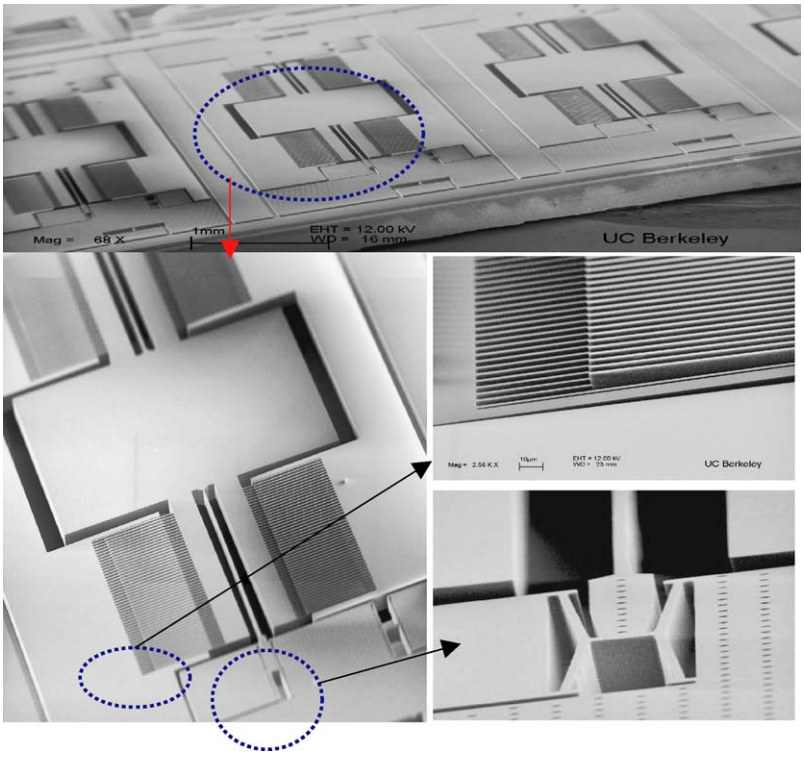

Fig. 8. SEM pictures of batch-fabricated torsional actuators with scanning mirrors by the selective stiction process.

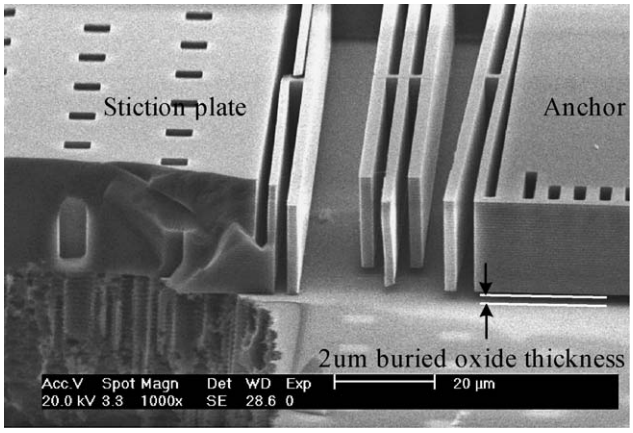

Fig. 9. Pictures of two types of torsional actuators and interdigitated self-aligned vertical comb fingers.

ric measurement of the device shown in Fig. 8 and the measured initial tilt angle of the rotor is 1.05°. It is also observed that the stiction-plates are completely flat after the stiction process.

4. Experimental characterization of device performance and reliability

The dynamic performance of the actuator is measured and presented in Fig. 11. Data were collected using 19 V_{dc} and 15 V_{pp} drive on an angular vertical comb actuator with a mirror. The resonant frequency is measured at 920 Hz, and a maximum optical scanning angle of 85° is achieved. The nonlinear frequency response [13] is supposed to be from the large angular motion of the actuator. The measured quality factor is 162 in air.

To ensure the reliability of the stiction-plate and the operational stability of the fabricated actuator, we drove the device at its resonance for 252 h. The resonant frequency and scanning angle values measured at every 12 h are plotted in Fig. 12. This corresponds to total 835 million cycles of operation, and during which the resonance drift is smaller than 0.15% for the center frequency and 2.3% of the peak amplitude. It is not obvious if this variation is from the degradation of the device or from other possible effects such as unstable voltage source. However, considering this very small amount of variation, the scanning mirror actuators made by selective stiction method are robust and reliable.

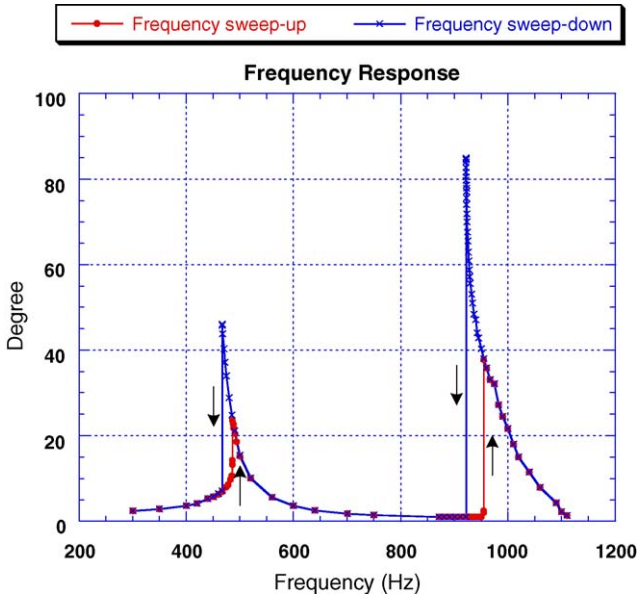

Fig. 11. Frequency response of the microactuator.

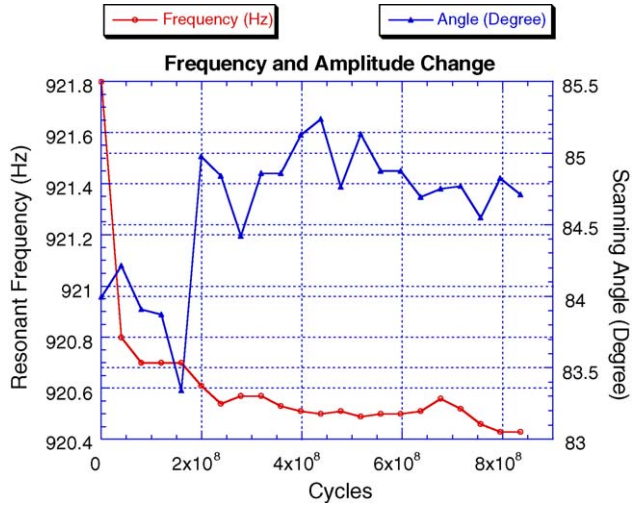

Fig. 12. Measured scanning angle and resonant frequency of the microactuator over 835 million cycles.

5. Conclusion

Selective stiction of silicon microstructures was successfully applied to build angular vertical comb actuators in a batch pro-

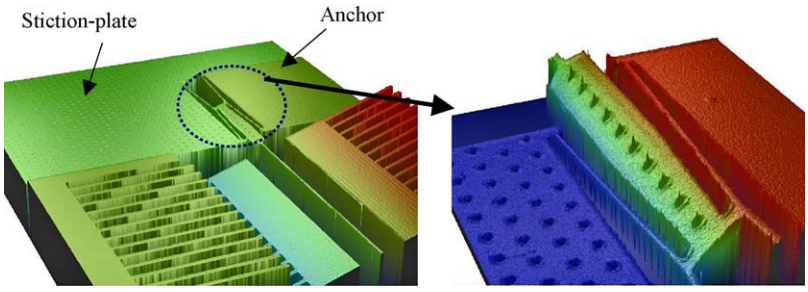

Fig. 10. White light interferometric measurement of the angular vertical comb actuator.

cess that is the simplest fabrication method known for this type of microdevices. The manufacturing process presented in this work is so far the simplest method known to fabricate vertically driven comb-actuators. Novel design for stiction-plate springs was presented to minimize unnecessary compliances in unwanted direction and yet giving enough compliance for the stiction-plate to get stuck down easily to the substrate during the fabrication process. The effect of this stiction-spring was evaluated by the vibration modal analysis of the rotor, and the result showed negligible addition of the total compliance of the moving part. The measured dynamic performance of the actuator showed very large angular motion at low drive voltage. The prototype microactuators operate at a resonant frequency of 0.92 kHz with 85° optical scanning angle and quality factor of 162 in air under driving voltages of 19 V_{dc} plus 15 V_{pp}. A reliability test on an unpackaged actuator with more than 800 million cycles of operation showed extremely small variation in the resonant frequency and scanning angle, showing no sign of degradation in the induced stiction interface or the microstructures.

Acknowledgement

The devices were fabricated in the UC-Berkeley Microfabrication Laboratory. The author thanks to Dr. Ben Costello for the inspiring discussion on spring design.

References

[1] J.A. Yeh, H. Jiang, N.C. Tien, Integrated polysilicon and DRIE bulk silicon micromachining for an electrostatic torsional actuator, J. Microelectromechanical Syst. 8 (4) (1999) 456–465.

[2] R.A. Conant, J.T. Nee, K. Lau, R.S. Mueller, "A Flat High-Frequency Scanning Micromirror", 2000 Solid-State Sensor and Actuator Workshop, Hilton Head, SC, pp. 6–9.

[3] U. Krishnamoorthy, D. Lee, O. Solgaard, Self-aligned vertical electrostatic combdrives for micromirror actuation, J. Microelectromechanical Syst. 12 (4) (2003) 458–464.

[4] P.R. Patterson, D. Hah, H. Nguyen, H. Toshiyoshi, R.M. Chao, M.C. Wu, A scanning micromirror with angular comb drive actuation, in: 15th IEEE International Conference on Micro Electro Mechanical Systems, 2002, pp. 544–547.

[5] H. Xie, Y. Pan, G.K. Fedder, A CMOS-MEMS mirror with curled-hinge comb drives, J. Microelectromechanical Syst. 12 (4) (2003) 450–457.

[6] J. Kim, H. Choo, L. Lin, R.S. Muller, Microfabricated Torsional Actuator by Self-Aligned Plastic Deformation, The 12th International Conference on Solid-State Sensors, Actuators Microsyst. (2003) 1015–1018.

[7] J. Kim, L. Lin, Batch-Fabricated Scanning Micromirrors Using Localized Plastic Deformation of Silicon, 17th Annual IEEE International Micro Electro Mechanical Systems Conference, pp. 494–497.

[8] R. Maboudian, R.T. Howe, Critical review: adhesion in surface micromechanical structures, J. Vacuum Sci. Technol. B 15 (1) (1997) 1–20.

[9] C.H. Mastrangelo, C.H. Hsu, Mechanical stability and adhesion of microstructures under capillary forces. I. Basic theory, J. Microelectromechanical Syst. 2 (1) (1993) 33–43.

[10] S.M. Ali, L.M. Phinney, Investigation of adhesion during operation of MEMS cantilevers, in: SPIE-Int. Soc. Opt. Eng. Proceedings of the International Society for Optical Engineering, vol. 5343, no. 1, 2003, pp. 215–226.

[11] J. Kim, D. Christensen, L. Lin, "Selective Stiction Based Vertical Comb Actuators," 18th Annual IEEE International Micro Electro Mechanical Systems Conference (MEMS-2005), pp. 403–406.

[12] P.J. Resnick, P.J. Clews, Whole wafer critical point drying of MEMS devices, in: SPIE-Int. Soc. Opt. Eng. Proceedings of the International Society for Optical Engineering, vol. 4558, 2001, pp. 189–196.

[13] AliH. Nayfeh, DeanT. Mook, Nonlinear Oscillations, Wiley-Interscience, NY, 1979, pp. 6–11.